UNIVERSITY OF LEEDS

This is a repository copy of *Micro-mechanical homogenisation of three-leaf masonry walls under compression*.

White Rose Research Online URL for this paper:
https://eprints.whiterose.ac.uk/179173/

Version: Accepted Version

Article:

Drougkas, A orcid.org/0000-0002-8647-9993 and Sarhosis, V orcid.org/0000-0002-8604-8659 (2021) Micro-mechanical homogenisation of three-leaf masonry walls under compression. Engineering Structures, 245. 112890. ISSN 0141-0296

https://doi.org/10.1016/j.engstruct.2021.112890

© 2021, Elsevier. This manuscript version is made available under the CC-BY-NC-ND 4.0 license http://creativecommons.org/licenses/by-nc-nd/4.0/.

Reuse

This article is distributed under the terms of the Creative Commons Attribution-NonCommercial-NoDerivs (CC BY-NC-ND) licence. This licence only allows you to download this work and share it with others as long as you credit the authors, but you can't change the article in any way or use it commercially. More information and the full terms of the licence here: https://creativecommons.org/licenses/

Takedown

If you consider content in White Rose Research Online to be in breach of UK law, please notify us by emailing eprints@whiterose.ac.uk including the URL of the record and the reason for the withdrawal request.

White Rose
university consortium
Universities of Leeds, Sheffield & York

eprints@whiterose.ac.uk
https://eprints.whiterose.ac.uk/

Micro-mechanical homogenisation of three-leaf masonry walls under compression

Anastasios Drougkas[1], Vasilis Sarhosis

School of Civil Engineering, University of Leeds, Woodhouse Lane, LS2 9JT, Leeds, United Kingdom

Abstract

Three-leaf masonry panels are typically composed of external leaves of irregularly bonded units and a rouble infill. The complexity of the response of these structures to mechanical loading arises from: a) the interaction of the leaves and b) the irregularity of the bond pattern of the outer leaves. This complexity makes analytical and computational modelling of these structures difficult and costly, respectively.

This paper proposes a computational approach for the calculation of the mechanical properties of the three-leaf masonry from the properties of its constituent materials and its geometry. Using micro-mechanical analysis approaches applied in composite materials and accounting for the interaction of the leaves through a simple analytical approach, the homogenised elastic stiffness and strength of a representative volume element of three-leaf masonry can be calculated with very low computational cost.

The analysis method is validated against experimental results from the literature. It is found that the proposed model provides accurate results for a relatively wide range of case studies. These results are expanded upon through a sensitivity study, highlighting the most important material and geometric parameters influencing the predicted compressive strength of three-leaf masonry walls.

Keywords

masonry – micro-mechanics – damage mechanics – homogenisation – multi-scale modelling

[1] Corresponding author: A.Drougkas@leeds.ac.uk

1 Introduction

Three-leaf masonry construction is a very common structural typology, strongly linked with both architectural heritage and vernacular construction. It is typically composed of two external leaves made of regularly or, more frequently, irregularly bonded stone or brick masonry and an inner leaf made of low cohesion, low strength materials, including loose mortar, soil and stone or brick fragments. Three-leaf masonry is a highly heterogeneous structure, composed of macroscopically distinguishable material phases and leaves with widely different mechanical properties [1]. Failure in these structures under mechanical loading may occur due to separation of poorly interlocked leaves, out-of-plane collapse or failure of the materials in tension, shear or compression. Load transfer between the material phases and between the distinct leaves, which governs the developed stresses within each constituent material, depends on numerous mechanical and geometric properties characterising the three-leaf structure and the connectivity of the leaves [2].

Experimental campaigns characterising the mechanical properties of three-leaf masonry, accompanied by comprehensive characterisation of the individual materials, are relatively few [2–6]. Despite the limited number of such studies, the results are enlightening in terms of describing the failure mode and the salient characteristics of the response. These studies typically include the determination of the Young's modulus and compressive strength, the measurement of the effects of grouting or other strengthening measures on capacity and the investigation of the interaction between leaves [1].

A variety of models for three-leaf masonry has been proposed in the literature. Analytical expressions for predicting the compressive strength [6–9] have been calibrated, relying partly on the mechanical properties of the materials and partly on empirical or semi-empirical observations or qualitative assessments of leaf interlocking. Further, computational modelling using finite elements has been attempted [2,10], this approach being very case-specific and characterised by high computational cost and modelling effort. Finally, method-of-cells approaches have been successfully applied for the analysis of both single-leaf [11] and multi-leaf masonry structures [12].

A very promising approach for the analysis of the external leaves of three-leaf masonry is treating the outer leaf as a composite material consisting of a mortar matrix with stone or brick unit inclusions. This approach is suitable for providing averaged values of stresses in the components of a composite material and for calculating the homogenised properties of the material with low computational cost. In the initially studied case of a composite material consisting of particle inclusions in a matrix, it is possible to relate the stresses within the inclusion to a given applied stress in an infinite matrix [13]. This model was later extended to account for composite materials with tightly packed inclusions and the interaction between them and with the surrounding matrix [14,15], a condition more closely resembling that encountered in the external leaves of masonry structures. While the shape of the inclusions is often considered to be ellipsoidal, and despite solutions of the problem existing for near-rectangular inclusions [16], this modelling approach has been applied in linear elastic modelling masonry structures with ellipsoidal inclusions approximating cuboid brick units with good accuracy [17]. Finally, nonlinear analyses of cements and mortar using this micro-mechanical approach have been successful in capturing the behaviour of brittle materials [18–21], providing a basis for application on masonry structures.

In this paper a model for the calculation of the elastic properties of three-leaf masonry structures is proposed. This goal is accomplished through a combined use of micro-mechanical modelling and analytical expressions for the homogenisation of the external leaf and the simulation of leaf interaction, respectively. This approach allows for the calculation of mechanical properties, primarily of the compressive strength, as a function of the geometric disposition and mechanical properties of the primary components comprising the three-leaf structure: units, mortar and fill material. Simultaneously, the coupled use of micro-mechanics and analytical expressions keeps the computational cost of non-linear analysis low.

The accuracy of the model is validated against experimental data involving compression tests on three-leaf masonry members. Only case studies with sufficient material characterisation are considered in this validation in order to minimise the number of assumptions concerning unknown material properties. Finally, a sensitivity study is performed for identifying the geometric and material parameters that have the strongest effect on the compressive strength of the masonry. This investigation can serve as a guide for future characterisation efforts in the study of three-leaf masonry structures through the identification of the most crucial material parameters.

2 Two-scale micro-mechanical model

2.1 Overview

The proposed model deals with the simulation of three-leaf masonry structures under mechanical loading. At the macro-scale, the structure consists of two outer leaves and an enclosed inner leaf. The outer leaves are composed of masonry units and mortar joints, while the inner leaf is composed of stone or brick fragments embedded in a highly porous fill material; the latter often being the same material as the mortar in the joints but less compacted. In the present study, it is considered that the inner and outer leaves are connected through a plane interface, thus not explicitly considering the potential presence of keyed collar joints. A visual representation of a representative three-leaf masonry structure is given in Figure 1.

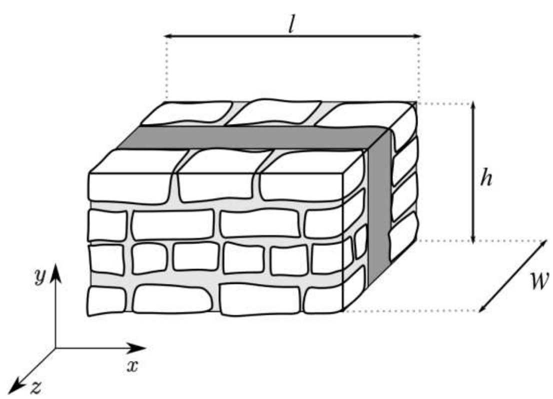

Figure 1 General layout of three-leaf masonry structure featuring units of different sizes.

The modelling strategy consists in the serial two-scale analysis of three-leaf masonry walls. At the micro-scale, the interaction of the components within the leaves is modelled for deriving the stresses and strains at each material phase. At the macro-scale the interaction of the outer and inner leaves is modelled. The two scales are solved separately and coupled for deriving the homogenised stresses and strains of the masonry [22].

2.2 Homogenisation of masonry leaves

The outer leaves of a three-leaf masonry are treated as a composite material consisting of stone or brick unit inclusions in a mortar matrix. In this context, an inclusion is defined as a region embedded in an infinite, homogeneous and isotropic matrix. When the matrix undergoes a change in size and shape, the inclusion in turn undergoes a deformation which is different from that of the matrix, assuming the two phases possess different material properties. Defining the eigenstrain $\boldsymbol{\varepsilon}^*$ as the strain state within the inclusion upon removal of the constraint provided to it by the matrix, the strain within the inclusion is equal to:

$$\varepsilon_{ij} = S_{ijkl}\varepsilon^*{}_{kl} \tag{1}$$

where S_{ijkl} are the components of Eshelby's tensor $\boldsymbol{S}$. These components are a function of the shape of the inclusion, with ellipsoidal inclusions having received the most attention in the literature. The outer surface of an ellipsoid is defined by the equation:

$$\frac{x^2}{a_1{}^2} + \frac{y^2}{a_2{}^2} + \frac{z^2}{a_3{}^2} = 1 \tag{2}$$

where a_1, a_2 and a_3 are the half-length, half-height and half-width of the ellipsoid. These ellipsoids are used for approximating the shape of units in the outer leaves, be they of cuboid or more rounded shape. This approximation of cuboids with ellipsoids does not appear to lead to any marked difference between computed elastic properties of the masonry and experimentally derived values [17,23]. An ellipsoidal inclusion is illustrated in Figure 2.

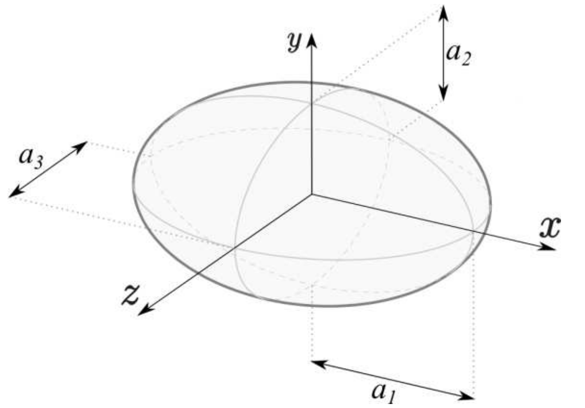

Figure 2 Illustration of an ellipsoidal inclusion.

For ellipsoidal inclusions, with their axes as shown in Figure 2 aligned with the axes of the masonry as shown in Figure 1, the components of Eshelby's tensor $\boldsymbol{S}$ are calculated as [24]:

$$\begin{aligned} S_{1111} &= \frac{3}{8\pi(1-\nu)} {a_1}^2 I_{11} + \frac{1-2\nu}{8\pi(1-\nu)} I_1 \\ S_{1122} &= \frac{1}{8\pi(1-\nu)} {a_2}^2 I_{12} + \frac{1-2\nu}{8\pi(1-\nu)} I_1 \\ S_{1133} &= \frac{1}{8\pi(1-\nu)} {a_3}^2 I_{13} + \frac{1-2\nu}{8\pi(1-\nu)} I_1 \\ S_{1212} &= \frac{{a_1}^2 + {a_2}^2}{16\pi(1-\nu)} I_{12} + \frac{1-2\nu}{16\pi(1-\nu)} (I_1 + I_2) \end{aligned} \tag{3}$$

following the symmetries:

$$S_{ijkl} = S_{jikl} = S_{ijlk} \tag{4}$$

and ν being the Poisson's ratio of the matrix. The parameters I_i and I_{ij} are calculated by the elliptical integrals [25]:

$$I_1 = 2\pi a_1 a_2 a_3 \int_0^\infty \frac{ds}{({a_1}^2 + s)\Delta(s)} \tag{5}$$

$$I_{11} = 2\pi a_1 a_2 a_3 \int_0^\infty \frac{ds}{({a_1}^2 + s)^2 \Delta(s)}$$

$$I_{12} = 2\pi a_1 a_2 a_3 \int_0^\infty \frac{ds}{({a_1}^2 + s)({a_2}^2 + s)\Delta(s)}$$

where:

$$\Delta(s) = \sqrt{({a_1}^2 + s)({a_2}^2 + s)({a_3}^2 + s)} \qquad (6)$$

The remaining parameters I_i and I_{ij} are calculated by cyclic permutation through subscripts 1,2,3.

Instead of a single inclusion, we can consider a composite material C comprised of n inclusion groups i within a matrix m. Each group represents inclusions with the same dimensions and material properties. The dilute estimate $\boldsymbol{T}_i$ of the i-th inclusion group is equal to:

$$\boldsymbol{T}_i = [\boldsymbol{I} + \boldsymbol{S}_i \boldsymbol{C}_m^{-1}(\boldsymbol{C}_i - \boldsymbol{C}_m)]^{-1} \qquad (7)$$

where $\boldsymbol{I}$ is the identity tensor and $\boldsymbol{C}_m$ and $\boldsymbol{C}_i$ are the stiffness tensors of the matrix and the inclusion respectively. The matrix strain concentration factor $\boldsymbol{A}_C$ in the composite is equal to:

$$\boldsymbol{A}_C = \left(\omega_m \boldsymbol{I} + \sum_{i=1}^{n} \omega_i \boldsymbol{T}_i \right)^{\boldsymbol{-1}} \qquad (8)$$

where ω_i is the volume ratio of the i-th group of inclusions and ω_m the volume ratio of the matrix, both with respect to the total volume of the composite. The strain concentration tensor $\boldsymbol{A}_i$ of the i-th inclusion group in the composite material is equal to:

$$\boldsymbol{A}_i = \boldsymbol{T}_i \boldsymbol{A}_C \qquad (9)$$

Finally, the effective stiffness tensor $\boldsymbol{C}_C$ of the composite material is [26]:

$$\boldsymbol{C}_C = \boldsymbol{C}_m + \sum_{i=1}^{n} \omega_i (\boldsymbol{C}_i - \boldsymbol{C}_m) \boldsymbol{A}_i \tag{10}$$

The strain in the matrix $\boldsymbol{\varepsilon}_m$ is equal to [14]:

$$\boldsymbol{\varepsilon}_m = \boldsymbol{A}_C \boldsymbol{\varepsilon}_C \tag{11}$$

where $\boldsymbol{\varepsilon}_C$ is the macroscopic strain in the composite, while the stress $\boldsymbol{\sigma}_m$ in the matrix is equal to:

$$\boldsymbol{\sigma}_m = \boldsymbol{C}_m \boldsymbol{\varepsilon}_m \tag{12}$$

The strain $\boldsymbol{\varepsilon}_i$ in the i-th group of inclusions is equal to [15]:

$$\boldsymbol{\varepsilon}_i = \boldsymbol{A}_i \boldsymbol{\varepsilon}_c \tag{13}$$

and the stress $\boldsymbol{\sigma}_i$ is equal to:

$$\boldsymbol{\sigma}_i = \boldsymbol{C}_i \boldsymbol{A}_i (\boldsymbol{C}_c)^{-1} \boldsymbol{\sigma}_C \tag{14}$$

where $\boldsymbol{\sigma}_C$ is the macroscopic stress in the composite.

Different unit inclusion groups in masonry are often clearly defined by the orientation of the units within the leaf. It is thus possible to distinguish between header, transversal or half-length header units depending on the bond type. Each of these types of units constitute an inclusion group. Brick masonry is often characterized by regularly sized units in the outer leaves, allowing the easy determination of the dimensions a_1, a_2 and a_3 for each inclusion group. This is not often the case in stone masonry, where the sizes of the units within the same inclusion group can vary noticeably. Due to this size irregularity, the dimensions a_1, a_2 and a_3 for each unit inclusion group are calculated as the volume-weighted average for each dimension in a given area in the masonry. Each average inclusion dimension $\langle a_i \rangle$ in direction i is equal to:

$$\langle a_i \rangle = \frac{\sum a_i \cdot V}{\sum V} \tag{15}$$

with V being the volume of each individual unit in the studied area of masonry. This approach ensures that the average dimension is controlled by the dimension of the units occupying the greatest volume in the leaf. For masonries with highly irregular texture, the calculation of the average dimensions can be performed for different sections of the masonry, resulting in the calculation of different mechanical properties in each section.

This homogenization process can be applied in a straightforward manner for the outer leaves: the mortar acts as the matrix and the units as the inclusions. The geometry and volume ratio of the units can be determined relatively easily through visual or photogrammetric inspection. The same process can in principle be adopted for the inner leaf as well, considering the fill material as the matrix and the various fragments as the inclusions. Additionally, pores can be included in the inner leaf in the form of zero-stiffness inclusions. However, using this approach for the inner leaf is deemed impractical due to the typical absence of accurate geometric data for the components of the inner leaf, the difficulty in acquiring such data from inspection, as opposed to the case of the outer leaves, and from the fact that the inner leaf is often characterised mechanically as a whole in experimental campaigns. Therefore, the inner leaf is here treated for the most part as a homogeneous material.

2.3 Masonry leaf interaction

The interaction of the masonry leaves is accounted for through a method-of-cells approach for the analysis of a representative volume element (RVE) of masonry [12]. In this context, the interaction is modelled through simple analytical expressions of stress equilibrium and strain compatibility between the inner leaves I and outer leaves O for calculating the elastic properties of the masonry M. Focusing on normal applied stresses, and having considered a plane interface between the leaves, shear stresses and strains are disregarded as these, due to the boundary conditions, do not develop in the RVE when it is subjected to normal stresses/strains only.

Strain compatibility between the leaves dictates that both leaves deform equally in the longitudinal (x) and vertical (y) direction leading to the strain equalities:

$$\varepsilon_0^{(xx)} = \varepsilon_I^{(xx)} = \varepsilon_M^{(xx)}$$

$$\varepsilon_0^{(yy)} = \varepsilon_I^{(yy)} = \varepsilon_M^{(yy)} \tag{16}$$

In the transversal (z) direction, the strain of the masonry is defined as:

$$\varepsilon_M^{(zz)} = \omega_O \varepsilon_O^{(zz)} + \omega_I \varepsilon_I^{(zz)} \tag{17}$$

where ω_O and ω_I are, respectively, the volume ratios of the outer and inner leaves with respect to the total volume of the masonry.

Stress equilibrium in the horizontal and vertical directions is expressed as:

$$\sigma_M^{(xx)} = \omega_O \sigma_O^{(xx)} + \omega_I \sigma_I^{(xx)}$$

$$\sigma_M^{(yy)} = \omega_O \sigma_O^{(yy)} + \omega_I \sigma_I^{(yy)} \tag{18}$$

while stress equality between leaves in the transversal direction is expressed as:

$$\sigma_M^{(zz)} = \sigma_O^{(zz)} = \sigma_I^{(zz)} \tag{19}$$

The above conditions amount to an iso-strain assumption in the vertical and horizontal direction and an iso-stress assumption in the transversal direction [27]. These conditions, along with Hooke's law for the inner and outer leaves, can be expressed in a more convenient tensor form as follows:

$$\begin{bmatrix} 0 \\ \vdots \\ 0 \\ \boldsymbol{\sigma}_M \\ \boldsymbol{\varepsilon}_M \end{bmatrix} = \begin{bmatrix} (-\boldsymbol{C}_I)^{-1} & \boldsymbol{I} & \boldsymbol{0} & \boldsymbol{0} \\ \boldsymbol{0} & \boldsymbol{0} & (-\boldsymbol{C}_O)^{-1} & \boldsymbol{I} \\ \boldsymbol{K}_1 & \boldsymbol{0} & \boldsymbol{K}_3 & \boldsymbol{0} \\ \boldsymbol{0} & \boldsymbol{K}_2 & \boldsymbol{0} & \boldsymbol{K}_4 \end{bmatrix} \cdot \begin{bmatrix} \boldsymbol{\sigma}_I \\ \boldsymbol{\varepsilon}_I \\ \boldsymbol{\sigma}_O \\ \boldsymbol{\varepsilon}_O \end{bmatrix}$$

$$\boldsymbol{K}_1 = \begin{bmatrix} \omega_I & 0 & 0 \\ 0 & \omega_I & 0 \\ 0 & 0 & 1 \end{bmatrix}, \boldsymbol{K}_2 = \begin{bmatrix} 1 & 0 & 0 \\ 0 & 1 & 0 \\ 0 & 0 & \omega_I \end{bmatrix}, \boldsymbol{K}_3 = \begin{bmatrix} \omega_O & 0 & 0 \\ 0 & \omega_O & 0 \\ 0 & 0 & 0 \end{bmatrix}, \boldsymbol{K}_4 = \begin{bmatrix} 0 & 0 & 0 \\ 0 & 0 & 0 \\ 0 & 0 & \omega_O \end{bmatrix} \tag{20}$$

where $\boldsymbol{0}$ is a 3×3 zero tensor, $\boldsymbol{I}$ is a 3×3 identity tensor and $\boldsymbol{C}_I$ and $\boldsymbol{C}_O$ are the stiffness tensors for the inner and outer leaves respectively. In the most general case of orthotropic inner and outer leaves, it is possible to derive closed-form expressions for all components of the orthotropic stiffness tensor $\boldsymbol{C}_M$ of the masonry (defined as $\boldsymbol{\sigma}_M = \boldsymbol{C}_M \boldsymbol{\varepsilon}_M$) from eq. (20) as a function of the components of the $\boldsymbol{C}_I$ and $\boldsymbol{C}_O$ tensors. The expressions involving components in the out-of-plane (z) direction are tediously long, but the remainder are relatively simple and more relevant for structural analysis. The horizontal Young's modulus $E^{(x)}$ of the masonry reads:

$$E^{(x)} = \frac{\omega_I E_I^{(x)} \left[\omega_I E_I^{(y)} \left(\nu_O^{(xy)} \nu_O^{(yx)} - 1\right) + \omega_O E_O^{(y)} \left(\nu_I^{(yx)} \nu_O^{(xy)} - 1\right)\right] + \omega_O E_O^{(x)} \left[\omega_I E_I^{(y)} \left(\nu_I^{(xy)} \nu_O^{(yx)} - 1\right) + \omega_O E_O^{(y)} \left(\nu_I^{(xy)} \nu_I^{(yx)} - 1\right)\right]}{\omega_I E_I^{(y)} \left(\nu_O^{(xy)} \nu_O^{(yx)} - 1\right) + \omega_O E_O^{(y)} \left(\nu_I^{(xy)} \nu_I^{(yx)} - 1\right)} \tag{21}$$

while the vertical Young's modulus $E^{(y)}$ can be obtained from eq. (21) by substitution between the x and y superscripts. The Poisson's ratio $\nu^{(xy)}$ is:

$$\nu^{(xy)} = \frac{\omega_I E_I^{(x)} \nu_I^{(yx)} \left(\nu_O^{(xy)} \nu_O^{(yx)} - 1\right) + \omega_O E_O^{(x)} \nu_O^{(yx)} \left(\nu_I^{(xy)} \nu_I^{(yx)} - 1\right)}{\omega_I E_I^{(x)} \left(\nu_O^{(xy)} \nu_O^{(yx)} - 1\right) + \omega_O E_O^{(x)} \left(\nu_I^{(xy)} \nu_I^{(yx)} - 1\right)} \tag{22}$$

while $\nu^{(yx)}$ can be obtained from eq. (22) by substitution between the x and y superscripts.

This model for the interaction of the leaves in the macro-scale can be used for the determination of the properties of a three-leaf masonry RVE. While it accounts for the in-plane interaction between the leaves through the iso-strain assumption, the iso-stress assumption in the transversal (z) direction cannot account for the out-of-plane effects caused by the bulging of the inner leaf under compression and the subsequent pushing-out of the outer leaf [2]. These out-of-plane effects arise as a consequence of structural element geometry and boundary conditions and thus cannot be captured through an RVE analysis. Conceptually, these effects can be modelled by treating the three-leaf structure as a bonded iso-strain composite under compression, infinitely thick in the longitudinal (x) direction [28], but this addition to the proposed model is not pursued in this paper. Finally, the model does not account for in-height differences of vertical deformation between the leaves, which is again an aspect arising at structural element level.

3 Calculation process

For the calculation of the compressive strength of the masonry, it is necessary to model the nonlinearity of the constituent materials of the composite. For compressive loading it is required to model the nonlinear response of the components in compression and tension. It has been previously determined numerically that interface nonlinearity between units and mortar has a negligible effect on the compressive strength of masonry [29]. Therefore, interfaces between inclusions and matrices are not considered in the present investigation.

A damage mechanics approach is adopted in this work, where the stiffness is reduced through multiplication with integrity variables in tension and compression. An exponential softening curve is adopted for the response in tension. The integrity variable in tension I_t is a function of the maximum principal strain ε^+ and the maximum principal effective stress σ_e^+. The principal strain ε^+ is calculated from the strain tensor of the inclusion or matrix being evaluated and the effective principal stress σ_e^+ is calculated from the stress tensor obtained by the product of the undamaged stiffness tensor and the strain tensor. The expression for the integrity variable reads [30]:

$$I_t(\varepsilon^+) = \begin{cases} 1 & 0 \le \varepsilon^+ \le \varepsilon_t \\ \dfrac{f_t}{\sigma_e^+} \exp\left(-\dfrac{f_t h}{G_t} (\varepsilon^+ - \varepsilon_t) \right) & \varepsilon_t \le \varepsilon^+ \end{cases} \tag{23}$$

where f_t is the tensile strength, G_t is the tensile fracture energy, h is the bandwidth and ε_t being the peak strain in tension, equal to:

$$\varepsilon_t = \frac{f_t}{E} \tag{24}$$

A parabolic curve is adopted for the materials in compression. The integrity variable in compression I_c is a function of the minimum principal strain ε^- and minimum principal effective stress σ_e^-, calculated similarly as in the case in tension, and is equal to [30]:

$$I_c(\varepsilon^-) = \begin{cases} 1 & \varepsilon_l \le \varepsilon^- \le 0 \\ -\dfrac{f_c}{\sigma_e^-} \dfrac{1}{3} \left(1 + 4 \dfrac{\varepsilon^- - \varepsilon_l}{\varepsilon_c - \varepsilon_l} - 2 \left(\dfrac{\varepsilon^- - \varepsilon_l}{\varepsilon_c - \varepsilon_l} \right)^2 \right) & \varepsilon_c \le \varepsilon^- \le \varepsilon_l \\ -\dfrac{f_c}{\sigma_e^-} \left(1 - \left(\dfrac{\varepsilon^- - \varepsilon_c}{\varepsilon_u - \varepsilon_c} \right)^2 \right) & \varepsilon_u \le \varepsilon^- \le \varepsilon_c \\ 0 & \varepsilon^- \le \varepsilon_u \end{cases} \tag{25}$$

where f_c is the compressive strength, ε_l is the limit of proportionality, equal to:

$$\varepsilon_l = -\frac{1}{3}\frac{f_c}{E} \tag{26}$$

with E being the Young's modulus, ε_c is the peak strain in compression, equal to:

$$\varepsilon_c = -\frac{5}{3}\frac{f_c}{E} \tag{27}$$

and ε_u is the ultimate strain, equal to:

$$\varepsilon_u = \varepsilon_c - \frac{3}{2}\frac{G_c}{f_c h} \tag{28}$$

where G_c is the compressive fracture energy and h is the bandwidth. In eq. (23) & (25) the bandwidth depends on the dimension of the component in the direction being evaluated. For example, for units in horizontal tension the bandwidth is equal to the length of the unit, while for bed joints in compression the bandwidth is equal to the thickness of the bed joint.

The combination of vertical compression and horizontal or transversal tension is common in units in masonry under vertical compression. The effect of lateral tension on the vertical compressive strength of the material is taken into account through a reduction of the initial compressive strength of the inclusions as a function of the lateral stress according to the expression:

$$f_c^*(\sigma) = \left(1 - \frac{\max\left(\sigma^{(xx)}, \sigma^{(zz)}, 0\right)}{f_t}\right) f_c \tag{29}$$

which is a very close linear approximation of a Mohr-Coulomb failure criterion in the tension-compression region.

Multi-axial compression of the inner leaf can result in the increase in its compressive strength. This increase is modelled through use of the Hsieh-Ting-Chen failure criterion [31]. When expressed in terms of principal stresses, the criterion reads:

$$f = A\frac{J_2}{{f_c}^2} + B\frac{\sqrt{J_2}}{f_c} + C\frac{\sigma_1}{f_c} + D\frac{I_1}{f_c} - 1 = 0 \tag{30}$$

where I_1 and J_2 are the first stress and second deviatoric stress invariants respectively and σ_1 is the maximum principal stress. The numerical parameters A, B, C and D are calibrated from uniaxial compression, uniaxial tension, biaxial compression and triaxial compression under equibiaxial stress. In the present study, the standard values originally reported by the authors of the criterion are used, although they can be calibrated experimentally for each studied case, albeit with some difficulty.

An isotropic damage approach is adopted for the reduction of the stiffness of the phases. The reduced stiffness tensor $\boldsymbol{C}^*$ of each matrix and inclusion is calculated as the product of the initial stiffness tensor $\boldsymbol{C}$ and the integrity variables:

$$\boldsymbol{C}^* = I_t(\varepsilon)\, I_c(\varepsilon)\, \boldsymbol{C} \tag{31}$$

In summary, the calculation sequence for each loadstep of a strain-driven nonlinear analysis is comprised of the following steps:

1. calculation of reduced stiffness tensors $\boldsymbol{C}^*$ of matrices and inclusions from eq. (31)
2. calculation of stiffness tensors $\boldsymbol{C}_I$ and $\boldsymbol{C}_O$ of inner and outer leaves from eq. (10)
3. increment of strain $\boldsymbol{\varepsilon}_M$ of masonry M
4. calculation of macroscopic stresses and strains in masonry M, inner leaf I and outer leaf O from eq. (20)
5. calculation of microscopic stresses and strains in matrices and inclusions within I and O from eq. (11) to (14)
6. calculation of integrity variables for next step from eq. (23) & (25)

The strain-driven analysis is continued until complete softening of the stress-strain curve of the composite is obtained. The calculated compressive strength of the composite is defined as the peak stress obtained. The calculation process is illustrated in the flowchart shown in Figure 3.

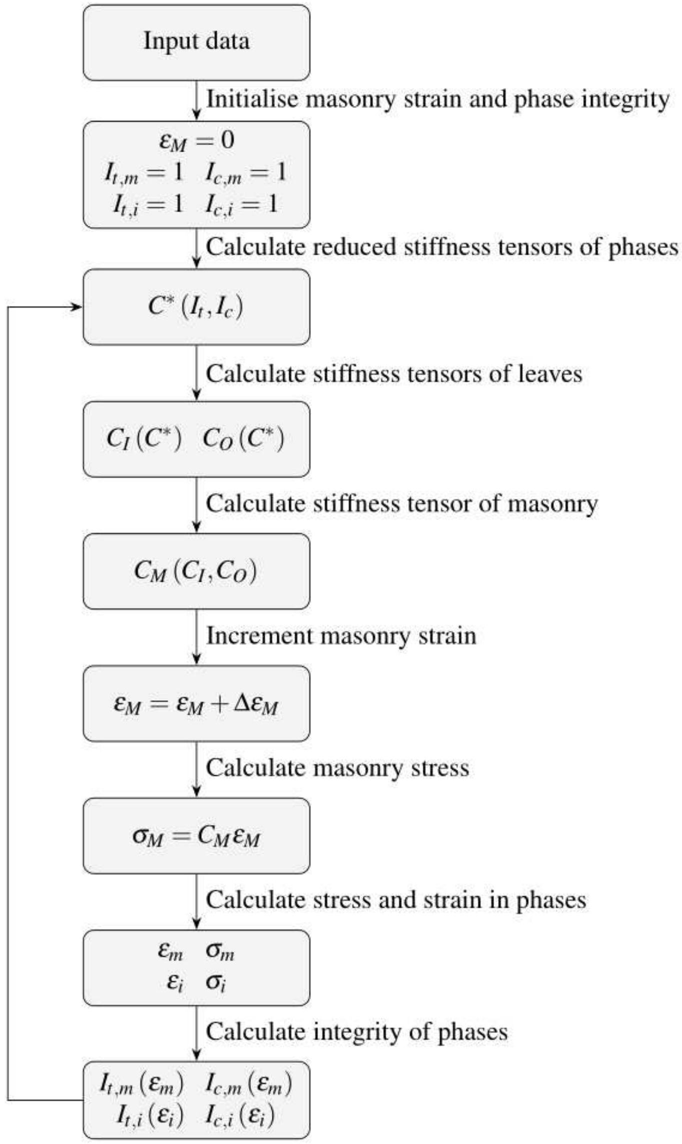

Figure 3 Flowchart of calculation process.

4 Model validation

The proposed model is validated against experimental data from the literature involving vertical compressive testing of three-leaf masonry. Only cases accompanied by extensive characterisation of the units, mortar and fill material were considered for analysis. Nevertheless, empirical assumptions were often necessary to fill in gaps in the mechanical characterisation, especially regarding the Young's moduli and Poisson's ratios of the constituent materials.

Geometric properties were derived from the case study description and from manual processing of the figures provided by the authors. When the relevant information is not available, empirical assumptions were made for certain material parameters based on statistical analysis of the available experimental inventory [29]. The Young's modulus E_u of the units was taken as 300 times the compressive strength and that of the mortar E_m and fill E_f as 700 times their respective compressive strength. The Poisson's ratio of the units ν_u was taken as 0.15 and that of the mortar ν_m 0.25 for simulating its significant lateral expansion near compressive yielding. Similarly, the Poisson's ratio of ungrouted fill ν_f was taken as equal to 0.10 due to its often high porosity, which decreases lateral expansion under vertical compression, while grouted fill was assigned a value of 0.20 for simulating the increase in cohesion after strengthening. The tensile strength of all components was taken as equal to 10% their respective compressive strength. The compressive fracture energy G_c is calculated for all components as [29]:

$$G_c = f_c d \tag{32}$$

were $d = 1$ mm and the tensile fracture energy G_t is calculated as [32]:

$$G_t = \frac{73 {f_c}^{0.18}}{1000} \tag{33}$$

4.1 Vintzileou & Tassios (1995)

This experimental campaign includes the compressive testing of three-leaf stone masonry wallettes subjected to vertical compression before and after grouting [6]. The outer leaf is built in single-wythe running bond, with alternate courses having slightly different embedment in the inner leaf, creating small keyed collar joints. Therefore, two types of units are distinguished. The compressive strength of the inner leaf after grouting is not reported. Therefore, only the case before grouting was used in this investigation.

4.2 Binda et al (2006)

In this case study masonry wallettes constructed of stone units, a strong mortar and a relatively cohesive inner leaf were tested in compression [2]. The outer leaf is composed of alternating courses of full- and half-length units. Two series of tests were conducted, each with a different geometry characterised by the presence or absence of a collar joint between leaves. In this simulation only the case without collar joints is simulated.

4.3 Vintzileou & Miltiadou-Fezans (2008)

The case study involves the compressive testing of masonry walls before and after grouting [5]. The properties of the fill after grouting were not reported. For simulating the wall after grouting, the compressive strength of the fill is assigned the target value reported by the authors despite this parameter not having been determined directly. The two outer leaves, both in single wythe construction, feature different geometric bond patterns. One leaf is composed of stone units in running bond, while the other features alternating courses of header stones and half-length stones. Both leaves feature horizontally and vertically arranged brick tiles, a feature typical of Byzantine architecture (cloisonné masonry) but lacking extensive characterisation in the literature. All these types of units are included in the model. Further, the stones feature different embedment lengths within the inner leaf. Nevertheless, the two outer leaves are considered identical in the model after averaging their featured geometric properties.

4.4 Oliveira et al (2012)

This series of experiments deals with the testing in compression of stone masonry before and after strengthening using grouting and other mechanical reinforcement methods [4]. The authors reported the mechanical properties of the fill after grouting, allowing the simulation of the compressive testing both before and after intervention.

4.5 Meimaroglou & Mouzakis (2018)

The case study involves the compressive testing of short stone masonry wallettes made using clay mortar [3]. The outer leaves were constructed in a running bond pattern consisting of full-length and half-length unit groups. The inner leaf was constructed using alternate layers of stone fragments and uncompacted mortar but was not the subject of mechanical characterisation itself. As such, in a departure from the methodology used in the other case studies simulated this paper, the properties of the fill were determined by applying the homogenisation method described in this paper.

4.6 Summary of case studies and numerical analysis results

All experimental data used for numerical analysis of the case studies are presented in Table 1, which includes all numerical parameters required for analysis, apart from the fracture energies which are calculated according to Eq. (32) and Eq. (33). The properties of the fill presented for the Meimaroglou & Mouzakis case were calculated numerically using the proposed model. These data are accompanied by the numerical analysis results using the proposed model in terms of vertical compressive strength, Young's modulus and in-plane Poisson's ratio.

Table 1 Experimental case study and numerical analysis results. Assumed values marked with an asterisk. Percentile difference between numerical and experimentally derived values in parentheses.

Component	Parameter	Symbol	[6]		[2]		[5]		[5]		[4]	[4]	[3]		Units
Unit	Length	l_u	293	293	310	150	300	180	300	180	172	172	320	160	mm
	Height	h_u	137	137	150	150	115	30	115	30	157	157	105	105	mm
	Width	w_u	130	140	170	170	155	140	155	140	99	99	165	165	mm
	Compressive strength	$f_{c,u}$	100	100	17.3	17.3	25	17	25	17	52.5	52.5	107.5	107.5	N/mm^2
	Tensile strength	$f_{t,u}$	10*	10*	1.8	1.8	2.5*	1.7*	2.5*	1.7*	5.25*	5.25*	3.1	3.1	N/mm^2
	Young's modulus	E_u	30000*	30000*	8525	8525	7500*	5100*	7500*	5100*	20600	20600	32250*	32250*	N/mm^2
	Poisson's ratio	ν_u	0.15*	0.15*	0.15*	0.15*	0.15*	0.15*	0.15*	0.15*	0.15*	0.15*	0.15*	0.15*	–
	Volume ratio	ω_u	0.425	0.425	0.380	0.551	0.667	0.133	0.667	0.133	0.850	0.850	0.652	0.185	–
Mortar	Joint thickness	t_m	10		10		20		20		20	20	20		mm
	Compressive strength	$f_{c,m}$	1.7		9.2		4.35		4.35		3.9	3.9	3.9		N/mm^2
	Tensile strength	$f_{t,m}$	0.17*		0.920*		0.435*		0.435*		0.39*	0.39*	0.39*		N/mm^2
	Young's modulus	E_m	1190*		6440*		3045*		3045*		410	410	2730*		N/mm^2
	Poisson's ratio	ν_m	0.25*		0.25*		0.25*		0.25*		0.25*	0.25*	0.25*		–
	Volume ratio	ω_m	0.150		0.069		0.200		0.200		0.150	0.150	0.185		–
Fill	Compressive strength	$f_{c,f}$	0.15		4.0		0.15		3.00		0.29	4.1	3.58		N/mm^2
	Tensile strength	$f_{t,f}$	0.015*		0.300*		0.015*		0.300*		0.029*	0.410*	0.487		N/mm^2
	Young's modulus	E_f	105*		1616		105*		900*		41	2870*	7134		N/mm^2
	Poisson's ratio	ν_f	0.10*		0.10*		0.10*		0.20*		0.10*	0.20*	0.13		–
Masonry	Length	l	600		310		1040		1040		600	600	700		mm
	Height	h	1200		790		1200		1200		1100	1100	550		mm
	Width	w	400		510		450		450		300	300	500		mm
	Inner leaf volume ratio	ω_I	0.325		0.333		0.275		0.275		0.333	0.333	0.333		–
	Outer leaf volume ratio	ω_O	0.675		0.667		0.725		0.725		0.667	0.667	0.667		–
	Compressive strength	f_c	1.49		5.81		1.94		3.49		2.00	3.60	4.00		N/mm^2
	Young's modulus	E	4611		1770		1313		1313		2122	2008	692		N/mm^2
Numerical results	Compressive strength	f_c	1.39 (-6.5%)		6.70 (15.3%)		3.43 (+76.9%)		3.62 (+3.6%)		2.84 (+42.2%)	3.44 (-4.3%)	4.26 (6.4%)		N/mm^2
	Young's modulus	E	7604 (+64.9%)		6128 (+246%)		4257 (+224%)		4474 (+241%)		3982 (+87.6%)	4929 (+145%)	12203 (+1663%)		N/mm^2
	Poisson's ratio	ν_{xy}	0.257		0.146		0.175		0.168		0.263	0.235	0.212		–

Overall, the model, coupled with the assumptions presented in the description of the calculation method, predicts the compressive strength of three-leaf masonry with good accuracy, despite some salient characteristics of three-leaf masonry having been omitted, primarily the out-of-plane effects caused by the boundary conditions. The model tends to overestimate the compressive strength, possibly due to the omission of out-of-plane effects. It is not currently clear whether the empirical assumptions regarding material parameters or whether elements of the modelling approach introduce a systematic bias on the model. The most notable lack of accuracy is that in the Vintzileou & Miltiadou-Fezans case before grouting [5], where the predicted compressive strength is 76.9% higher than the mean experimental value and 51% higher than the maximum experimental value. It is notable, however, that in the grouted case in the same experimental series, as in the cases investigated by Oliveira et al [4], the compressive strength is predicted with greater accuracy, indicating a mitigation of out-of-plane effects by the intervention. Since it is not clear which parameter has the strongest influence on the results, and since several material parameters were not directly characterised in the experimental campaign, this case will form the basis of a sensitivity study.

The proposed model and assumptions are less successful in predicting the Young's modulus of the three-leaf masonry case studies examined here even when the Young's moduli of the components were experimentally determined. The predicted Young's modulus is systematically higher than the experimentally derived value, especially in the Meimaroglou & Mouzakis case [3], where the difference is remarkable. It is noted for this case study that the value of the Young's modulus used for the units is very plausible for limestone of this strength [33], although the particulars of the limestone used are not known in detail. It is possible that imperfect compaction of the mortar in the joints and the presence of imperfections or voids in the inner leaf result in a reduction of the Young's modulus of masonry. Further, large differences between the empirically-derived and actual values of the Young's moduli of the components are a possible cause of this discrepancy. Consequently, the large differences between the computed and experimentally measured values highlight the need for comprehensive characterisation of all materials before application of the proposed model. Finally, it is currently unclear whether full simulation of the out-of-plane interaction of the leaves could reduce the calculated Young's modulus of masonry through the induction of bending on the outer leaf.

5 Sensitivity study

The object of the study is the sensitivity of compressive strength f_c, Young's modulus E and in-plane Poisson's ratio ν_{xy} of masonry to a set of material and geometric parameters. It is performed by variation of a) the Young's modulus and the Poisson's ratio of the stone and brick units (E_u, ν_u) and the mortar (E_m, ν_m), namely elastic material properties that are often not characterised in experimental campaigns due to practical difficulties in execution, b) the tensile f_t and compressive f_c strength of the fill, mortar and the stone and brick units (the tensile strength in often only indirectly characterized through flexural or splitting tests while the compressive strength of the fill is difficult to determine in existing structures), and c) the volume ratio ω_m of the mortar in the outer leaf and the length l_{u1} and height h_{u1} of the stone units, as these geometric parameters may vary substantially in different locations of irregular stone masonries or cannot be easily determined. Each parameter is varied without changing any of the others apart from the dimensions of the stone units, which are studied jointly. The Vintzileou & Miltiadou-Fezans [5] case is used for investigating elastic and geometric parameters and the Binda et al [2] case is used for investigating strength parameters, since the proposed model and assumptions were less successful in accurately predicting the compressive strength of the masonry in these two cases compared to the others. Additionally, the former case presents the opportunity of studying the influence of the brick tiling elements on the mechanical properties of cloisonné masonry. All material and geometric parameters in this section that have been normalized through division with the reference values found in Table 1 are represented using a hat operator, i.e. $\hat{f}_c$ is equal to the compressive strength of masonry calculated after variation of a parameter divided by the reference value of f_c. The parameters modified in the sensitivity study and the range of variation are presented in Table 2.

Table 2 Sensitivity study parameters and range of variation.

Component	Parameter	Symbol	Minimum	Maximum
Mortar	Young's modulus	$\hat{E}_m$	0.33	3.00
	Poisson's ratio	$\hat{\nu}_m$	0.60	1.20
	Compressive strength	$\hat{f}_{c,m}$	0.25	1.50
	Tensile strength	$\hat{f}_{t,m}$	0.25	1.50
	Content ratio	$\hat{\omega}_m$	0.25	1.75
Stone units	Young's modulus	$\hat{E}_{u1}$	0.33	3.00
	Poisson's ratio	$\hat{\nu}_{u1}$	0.33	1.33
	Compressive strength	$\hat{f}_{c,u1}$	0.25	1.50
	Tensile strength	$\hat{f}_{t,u1}$	0.25	1.50
	Length	$\hat{l}_{u1}$	0.25	2.00
	Height	$\hat{h}_{u1}$	0.25	2.00
Brick units	Young's modulus	$\hat{E}_{u2}$	0.33	3.00
	Poisson's ratio	$\hat{\nu}_{u2}$	0.33	1.33
Fill	Compressive strength	$\hat{f}_{c,f}$	0.25	1.50

The sensitivity of the calculated properties of masonry to elastic parameters of the components is illustrated in Figure 4. The influence of the Young's modulus E_m of mortar on the compressive strength f_c of masonry is notable. An decrease of E_m can result in an increase in f_c of up to nearly 20% due to higher confinement of the mortar. Additionally, lowering E_m increases the Poisson's ratio ν_{xy} of masonry, making the composite material more prone to lateral expansion under vertical compression. Lowering the Poisson's ratio ν_m of the mortar results in an increase in the predicted strength of masonry due to the development of lower lateral tensile stresses in the units. However, excessive reduction results in a decrease in the compressive strength. An increase in this parameter has the opposite effect on the units and leads to their tensile failure. It is noted that while ν_m can initially be very low due to porosity, it can increase rapidly near compressive failure of the mortar [34], which can in turn lead to premature failure of the masonry due to high tensile stresses in the units. Similarly, a higher Young's modulus E_{u1} of the stone units leads to more confinement of the mortar and an increase in the compressive strength of masonry, the overall effect being more pronounced compared to the variation of E_m. Increasing the Poisson's ratio ν_{u1} of the units makes their lateral deformation more compatible with the lateral expansion of the mortar, potentially decreasing lateral tensile stresses and reducing tensile damage. However, the effect is not particularly pronounced in this case study. Despite the low volume ratio of brick units, lowering the Young's modulus E_{u2} of brick can lead to a lower f_c due to increase in the stress concentration in the mortar. Finally, variation of the Poisson's ratio ν_{u2} of the brick does not strongly influence the calculated properties of the masonry.

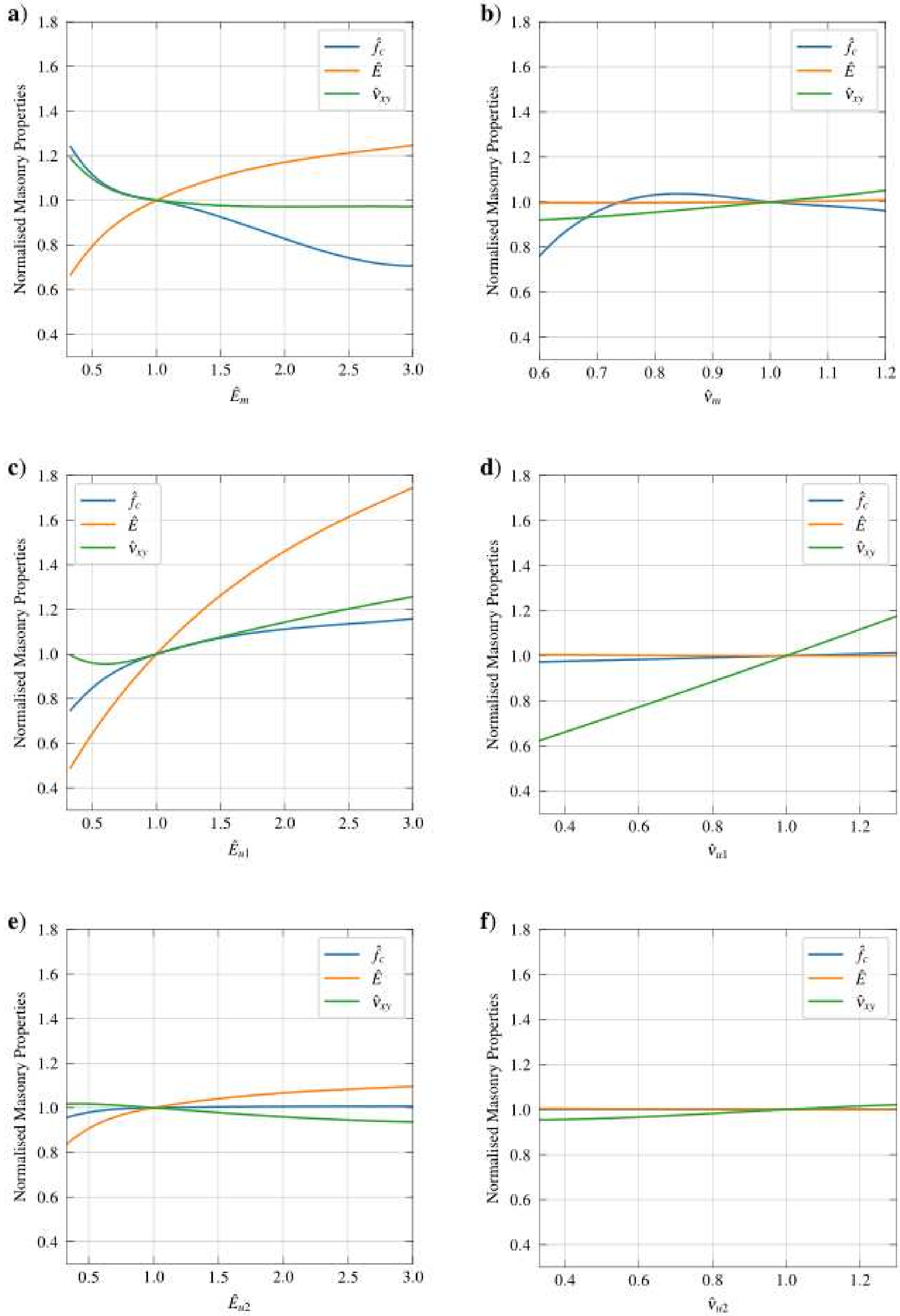

Figure 4 Results of sensitivity study on elastic parameters: a) Young's modulus of mortar, b) Poisson's ratio of mortar, c) Young's modulus of stone units, d) Poisson's ratio of stone units, e) Young's modulus of brick units and f) Poisson's ratio of brick units.

The sensitivity of the calculated properties of masonry to the tensile and compressive strength of the components is illustrated in Figure 5. For the investigated case, the calculated compressive strength f_c of masonry is insensitive to the tensile strength $f_{t,m}$ of the mortar due to the latter component being under confinement by the units. The compressive strength of masonry is not particularly sensitive to the tensile strength $f_{t,u1}$ of the stone units due to the low ratio of tensile over compressive stress developed in this component in this particular case. Different combinations of elastic properties for the mortar and units can lead to an increase in this ratio and result in sensitivity of the compressive strength of masonry to the tensile strength of the units. Further, existing local damage to the stone units, which would induce an apparent decrease in their tensile strength, could lead to a moderate reduction of the compressive strength of masonry.. The compressive strength f_c of the masonry is, as expected, not proportional to the compressive strength of the mortar and stone units. The compressive strength $f_{c,f}$ of the fill does not strongly affect the compressive strength of the masonry due to its very low stiffness, leading to the development of low compressive stresses in the fill.

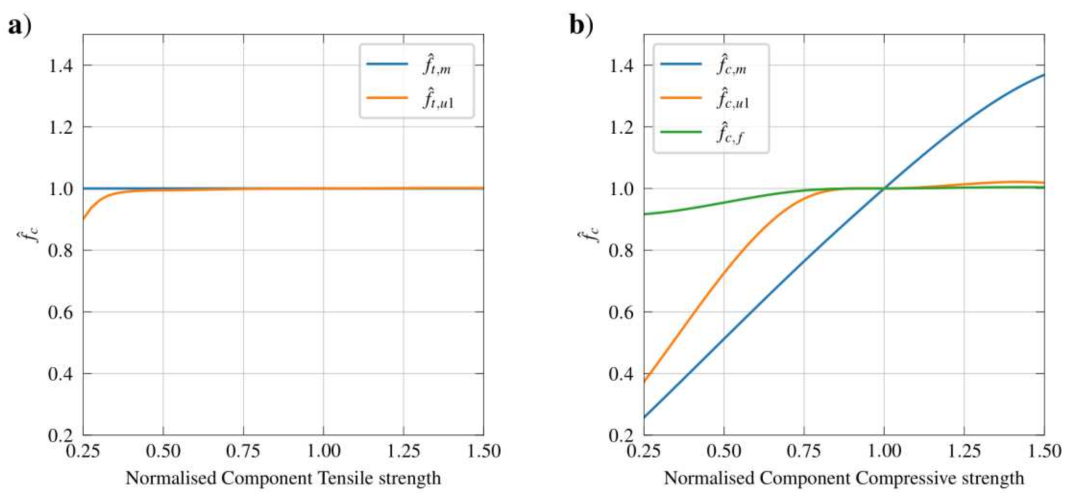

Figure 5 Results of sensitivity study on inelastic parameters: a) tensile strength and b) compressive strength of components.

The sensitivity of the calculated properties of masonry to geometric parameters is shown in Figure 6. While the compressive strength f_c of masonry is not particularly sensitive to the volume ratio ω_m of mortar, the Young's modulus E and Poisson's ratio v_{xy} of masonry are moderately influenced by ω_m. A higher mortar content increases the Poisson's ratio and decreases the Young's modulus of the masonry, resulting in a more deformable composite material. Higher deformability in sections of masonry with thicker mortar joints compared to adjacent sections can lead to deformation incompatibility, instability and loss of strength. Finally, the compressive strength of masonry shows notable sensitivity to the length l_{u1} and height h_{u1} of the stone units. The interaction of the parameters presents a complex profile. Overall, f_c is more sensitive to changes in height for a given length for a large proportion of the variation range studied, with shorter units typically yielding higher values of f_c. Units roughly 225 mm in length and 200 mm in height, a near-square shape which is encountered in one of the external leaves of the wall, result in substantially elevated values of f_c.

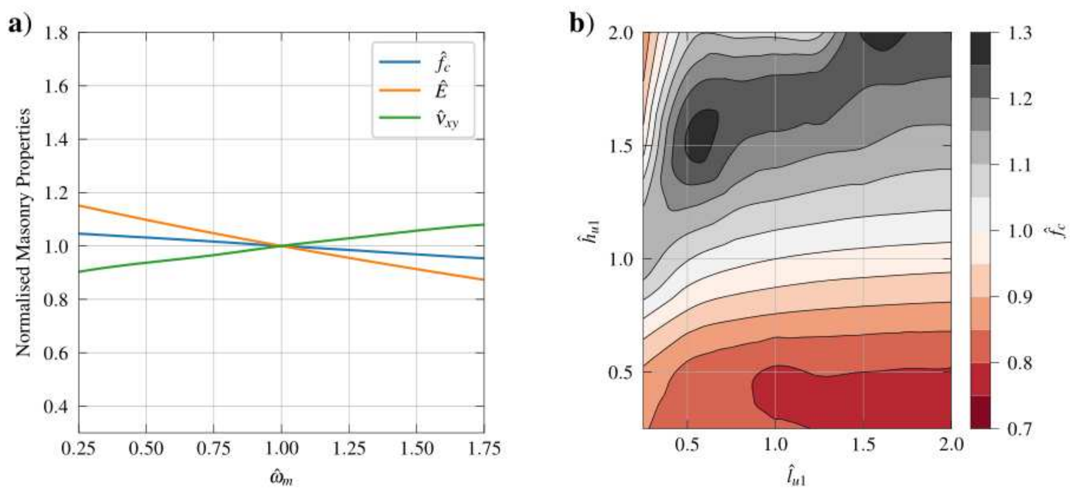

Figure 6 Results of sensitivity study on geometric parameters: a) volume ratio of mortar and b) length and height of units.

6 Conclusions

A method for the homogenisation of composite materials has been combined with a method-of-cells approach for the two-scale analysis of three-leaf masonry structures. It provides good accuracy in the prediction of the compressive strength of three-leaf masonry and highlights crucial characteristics of these structures with very low computational cost. The method requires a very dedicated approach in the mechanical characterisation of the unit, mortar and fill properties, but compensates for this requirement by providing an attractive alternative to finite element analysis for the determination of the mechanical properties of these structures. Finite element analysis necessarily suffers from the same requirement of rigorous material characterisation while inducing the additional burden of potentially very high computational cost. Further, the proposed method moves beyond currently available empirical models for three-leaf masonry under compression by proposing a degree of quantification of the problem typically not available in empirical models. Under this light, the advantages of micro-mechanical approaches of three-leaf masonry structures become apparent.

Following a sensitivity study using the proposed model, the compressive strength of masonry is found to be sensitive to properties such as the Poisson's ratio of the mortar, a parameter that is difficult to measure and presents significant nonlinearity. Additionally, the properties of secondary brick unit elements found in cloisonné masonry can moderately affect the calculated properties of masonry, making the characterisation of these elements a relevant task in the structural assessment of existing masonry structures. Therefore, the need for rigorous characterisation of the mechanical properties of all components becomes a pressing issue for the acquisition of accurate analysis results. Finally, variation in the dimensions of the units, which is common in stone masonry, strongly affects the calculated compressive strength. Therefore, geometric survey of the masonry texture, including the dimensions of the units, is shown to be an important aspect of structural assessment of masonry buildings.

The present work opens several potential avenues for future work. The interface between units and mortar can be included in an updated homogenisation process, which, coupled with failure models for interface tension and shear, can expand the modelling strategy here presented for the analysis of walls under in-plane shear. It is envisaged to complement this method with out-of-plane leaf interaction at the structural element scale for the analysis of complete masonry members through implementation of the updated micro-mechanics model in a finite element context. Evaluation of the results of an updated model can guide the adjustment of the modelling approach and the empirical assumptions accompanying it. Additionally, common mechanical strengthening measures, such as longitudinal and transversal ties can be modelled. Finally, the analysis method can be coupled with photogrammetry methods for the automatic acquisition of the geometry and calculation of the volume ratios and average dimensions of all components in the external leaves.

Acknowledgements

This work was funded by the EPSRC project "Exploiting the resilience of masonry arch bridge infrastructure: a 3D multi-level modelling framework" (ref. EP/T001348/1).

References

[1] Vintzileou E. Three-Leaf Masonry in Compression, Before and After Grouting: A Review of Literature. Int J Archit Herit 2011;5:513–38. https://doi.org/10.1080/15583058.2011.557137.

[2] Binda L, Pina-Henriques JL, Anzani A, Fontana A, Lourenço PB. A contribution for the understanding of load-transfer mechanisms in multi-leaf masonry walls: Testing and modelling. Eng Struct 2006;28:1132–48.

[3] Meimaroglou N, Mouzakis H. Mechanical properties of three-leaf masonry walls constructed with natural stones and mud mortar. Eng Struct 2018;172:869–76. https://doi.org/10.1016/j.engstruct.2018.06.015.

[4] Oliveira D V., Silva RA, Garbin E, Lourenço PB. Strengthening of three-leaf stone masonry walls: an experimental research. Mater Struct 2012;45:1259–76. https://doi.org/10.1617/s11527-012-9832-3.

[5] Vintzileou E, Miltiadou-Fezans A. Mechanical properties of three-leaf stone masonry grouted with ternary or hydraulic lime-based grouts. Eng Struct 2008;30:2265–76. https://doi.org/10.1016/j.engstruct.2007.11.003.

[6] Vintzileou E, Tassios TP. Three-leaf stone masonry strengthened by injecting cement grouts. J Struct Eng 1995;121:848–56. https://doi.org/10.1061/(ASCE)0733-9445(1995)121:5(848).

[7] Egermann R, Neuwald-Burg C. Assessment of the Load Bearing Capacity of Historic Multiple Leaf Masonry Walls. 10th Int. Brick Block Mason. Conf. Calgary, 1994, p. 1603–12.

[8] Silva B, Pigouni AE, Valluzzi MR, Modena C. Calibration of analytical formulations predicting compressive strength in consolidated three-leaf masonry walls. Constr Build Mater 2014;64:28–38. https://doi.org/10.1016/j.conbuildmat.2014.04.044.

[9] Valluzzi MR, Da Porto F, Modena C. Behavior and modeling of strengthened three-leaf stone masonry walls. Mater Struct 2004;37:184–92.

[10] Ramalho MA, Taliercio A, Anzani A, Binda L, Papa E. A numerical model for the description of the nonlinear behaviour of multi-leaf masonry walls. Adv Eng Softw 2008;39:249–57. https://doi.org/10.1016/j.advengsoft.2007.01.003.

[11] Milani G, Taliercio A. In-plane failure surfaces for masonry with joints of finite thickness estimated by a Method of Cells-type approach. Comput Struct 2015;150:34–51. https://doi.org/10.1016/j.compstruc.2014.12.007.

[12] Drougkas A, Roca P, Molins C. Analytical Micro-Modeling of Masonry Periodic Unit Cells – Elastic Properties. Int J Solids Struct 2015;69–70:169–88. https://doi.org/10.1016/j.ijsolstr.2015.04.039.

[13] Eshelby JD. The Determination of the Elastic Field of an Ellipsoidal Inclusion, and Related Problems. Proc R Soc Lond A Math Phys Sci 1957;241:376–96.

[14] Mori T, Tanaka K. Average stress in matrix and average elastic energy of materials with misfitting inclusions. Acta Metall 1973;21:571–4. https://doi.org/10.1016/0001-6160(73)90064-3.

[15] Benveniste Y. A new approach to the application of Mori-Tanaka's theory in composite materials. Mech Mater 1987;6:147–57. https://doi.org/10.1016/0167-6636(87)90005-6.

[16] Zou W, He Q, Huang M, Zheng Q. Eshelby's problem of non-elliptical inclusions. J Mech Phys Solids 2010;58:346–72. https://doi.org/10.1016/j.jmps.2009.11.008.

[17] Briccoli Bati S, Ranocchiai G, Rovero L. A micromechanical model for linear homogenization of brick masonry. Mater Struct 1999;32:22–30.

[18] Pichler B, Hellmich C, Eberhardsteiner J. Spherical and acicular representation of hydrates in a micromechanical model for cement paste: prediction of early-age elasticity and strength. Acta Mech 2008;203:137. https://doi.org/10.1007/s00707-008-0007-9.

[19] Pichler B, Hellmich C. Upscaling quasi-brittle strength of cement paste and mortar: A multi-scale engineering mechanics model. Cem Concr Res 2011;41:467–76.

https://doi.org/https://doi.org/10.1016/j.cemconres.2011.01.010.

[20] Esposito R, Hendriks MAN. A multiscale micromechanical approach to model the deteriorating impact of alkali-silica reaction on concrete. Cem Concr Compos 2016;70:139–52. https://doi.org/10.1016/j.cemconcomp.2016.03.017.

[21] Nežerka V, Zeman J, Němeček J. Micromechanics-based simulations of compressive and tensile testing on lime-based mortars. Mech Mater 2017;105:49–60. https://doi.org/10.1016/j.mechmat.2016.11.011.

[22] Geers MGD, Kouznetsova VG, Matouš K, Yvonnet J. Homogenization Methods and Multiscale Modeling: Nonlinear Problems. Encycl. Comput. Mech. Second Ed., American Cancer Society; 2017, p. 1–34. https://doi.org/10.1002/9781119176817.ecm2107.

[23] Briccoli Bati S, Ranocchiai G, Rovero L. Suitability of micromechanical model for elastic analysis of masonry. J Eng Mech 1999;125:922–9.

[24] Mura T. Micromechanics of Defects in Solids: Mechanics of Elastic and Inelastic Solids. 2nd ed. Springer Netherlands; 1987. https://doi.org/10.1007/978-94-009-3489-4.

[25] Routh EJ. Theorems on the attraction of ellipsoids for certain laws of force other than the inverse square. Philos Trans R Soc London Ser A 1895;186:897–950.

[26] Marzari N, Ferrari M. Textural and micromorphological effects on the overall elastic response of macroscopically anisotropic composites. J Appl Mech 1992;59:269–75. https://doi.org/10.1115/1.2899516.

[27] Alger MSM. Polymer Science Dictionary. 3rd ed. Springer; 2017. https://doi.org/10.1007/978-94-024-0893-5.

[28] Qiao S, Lu N. Analytical solutions for bonded elastically compressible layers. Int J Solids Struct 2015;58:353–65. https://doi.org/10.1016/j.ijsolstr.2014.11.018.

[29] Drougkas A, Roca P, Molins C. Numerical prediction of the behavior, strength and elasticity of masonry in compression. Eng Struct 2015;90:15–28.

https://doi.org/10.1016/j.engstruct.2015.02.011.

[30] Feenstra PH, De Borst R. A composite plasticity model for concrete. Int J Solids Struct 1996;33:707–30.

[31] Hsieh SS, Ting EC, Chen WF. A plastic-fracture model for concrete. Int J Solids Struct 1982;18:181–97.

[32] Federátion Internationale du Béton. The fib Model Code for Concrete Structures 2010. Wiley and Sons; 2013.

[33] Palchik V. On the Ratios between Elastic Modulus and Uniaxial Compressive Strength of Heterogeneous Carbonate Rocks. Rock Mech Rock Eng 2011;44:121–8. https://doi.org/10.1007/s00603-010-0112-7.

[34] Drougkas A, Verstrynge E, Hayen R, Van Balen K. The confinement of mortar in masonry under compression: Experimental data and micro-mechanical analysis. Int J Solids Struct 2019;162:105–20. https://doi.org/10.1016/j.ijsolstr.2018.12.006.